Journal of Magnetic Resonance 212 (2011) 378–385

Contents lists available at SciVerse ScienceDirect

Journal of Magnetic Resonance

journal homepage: www.elsevier.com/locate/jmr

High-pressure magic angle spinning nuclear magnetic resonance

David W. Hoyt, Romulus V.F. Turcu, Jesse A. Sears, Kevin M. Rosso, Sarah D. Burton, Andrew R. Felmy, Jian Zhi Hu *

Fundamental and Computational Sciences Directorate, Pacific Northwest National Laboratory, Richland, WA 99354, USA
Environmental Molecular Sciences Laboratory, Pacific Northwest National Laboratory, Richland, WA 99354, USA

ARTICLE INFO

Article history:
Received 20 June 2011
Revised 20 July 2011
Available online 31 July 2011

Keywords:
High-pressure MAS NMR
In situ NMR
CO_2
Carbon sequestration

ABSTRACT

A high-pressure magic angle spinning (MAS) NMR capability, consisting of a reusable high-pressure MAS rotor, a high-pressure rotor loading/reaction chamber for *in situ* sealing and re-opening of the high-pressure MAS rotor, and a MAS probe with a localized RF coil for background signal suppression, is reported. The unusual technical challenges associated with development of a reusable high-pressure MAS rotor are addressed in part by modifying standard ceramics for the rotor sleeve by abrading the internal surface at both ends of the cylinder. In this way, not only is the advantage of ceramic cylinders for withstanding very high-pressure utilized, but also plastic bushings can be glued tightly in place so that other removable plastic sealing mechanisms/components and O-rings can be mounted to create the desired high-pressure seal. Using this strategy, sealed internal pressures exceeding 150 bars have been achieved and sustained under ambient external pressure with minimal loss of pressure for 72 h. As an application example, *in situ* ^{13}C MAS NMR studies of mineral carbonation reaction intermediates and final products of forsterite (Mg_2SiO_4) reacted with supercritical CO_2 and H_2O at 150 bar and 50 °C are reported, with relevance to geological sequestration of carbon dioxide.

1. Introduction

Nuclear Magnetic Resonance (NMR) [1,2] is a powerful tool for obtaining detailed molecular structure and dynamics information of a system regardless of whether the system is in a solid, a liquid, a gaseous, or a supercritical state. A large number of NMR methods have been developed for addressing numerous chemical, physical and biological problems across scientific disciplines. Among them, the technique of magic angle spinning (MAS) [3,4] is one of the most widespread NMR methods and is the only technique that allows a high resolution NMR spectrum acquired on solids, semi-solids, or a heterogeneous system containing a mixture of solid, semi-solid, liquid and gaseous phases.

Despite its wide spread application, MAS under the condition of high-pressure, i.e., with pressure exceeding 70 bars, has not yet been reported although high pressure static NMR approaching kbar has been reported previously [5]. Technical challenges associated with high-pressure MAS are self-evident in the papers describing success at lower pressures. Sample cells cannot be made of any metals due to the strong eddy currents associated with a spinning metal in a strong magnetic field. This leaves only non-metals such as glasses, ceramics, and plastics as suitable materials for sample cells. Early efforts for developing high-pressure MAS NMR were focused on investigating the segmental motion of polymers that have been plasticized by dense gases [6–8]. The high-pressure cells in these studies used Pyrex glass tubes with an inner diameter (ID) of 3.4 mm and outer diameter (OD) of 5.85 mm. Gases were cryogenically transferred into the sample cell using standard volumetric absorption methods and then either flame sealed or epoxy sealed. The cell was then inserted into a 7.5 mm MAS spinner and balanced with KBr powder. Pressures of 40–70 bars were obtained in this manner using Xe and CO_2. The shortcomings of this method are that (i) reaction under a constant pressure becomes impossible, (ii) it is very difficult to exceed 70 bars of pressure due to the use of thin glass tubes, and (iii) it is impossible to re-open the cell to recharge and continue the reaction.

Later, a design based on the polymer Delrin™ having an internal high-pressure seal was reported by Yonker and Linehan [9], where the Delrin™ cell was a 3.3 mm ID by 11 mm OD cylinder that was inserted into a 13 mm ceramic MAS spinner after pressurization. Using this cell, a 94.2 MHz ^{19}F MAS spectrum of CH_3F at an initial pressure of 70 bars was acquired. But significant penetration of the CH_3F molecules into the Delrin™ materials, with a concomitant pressure reduction, was observed over time [9]. A similar penetration problem has been recently reported by Deuchande et al. [10], using CO_2 or N_2O in high-pressure MAS inserts made from the polymer PEEK. In the experiment of Deuchande et al. [10] the pres-

* Corresponding author at: Fundamental and Computational Sciences Directorate, Pacific Northwest National Laboratory, Richland, WA 99354, USA. Fax: +1 509 371 6546.
E-mail address: Jianzhi.Hu@pnnl.gov (J.Z. Hu).

1090-7807/$ - see front matter © 2011 Elsevier Inc. All rights reserved.
doi:10.1016/j.jmr.2011.07.019

sure was limited to 40 bars because a fast sample spinning rate of several kHz or more required the use of sample rotor with a small diameter, where it was very difficult to construct the sealing mechanism at high-pressure using the reported design. In addition to the problem of reaching high-pressure and the problem of penetration, another problem associated with the inserts made by polymers such as Delrin™ or PEEK is the strong unwanted carbon and/or proton background signal that may mask the signals associated with the investigation of a variety of systems containing carbon, or protons, or both.

To overcome most, if not all, of the problems associated with the prior designs and to extend the pressure well beyond 70 bars, in this work we use commercial ceramics as the sample rotor cylinder, and use plastics glued at both ends of the cylinder for a high-pressure seal that sets a new milestone. A localized RF coil design in a MAS NMR probe is used to minimize ^{13}C and ^{1}H background signals. A high-pressure loading chamber is also designed that is capable of sealing *in situ*, and re-opening of the valve on the HP-MAS-R enabling sample access at pressure for continued reaction and reanalysis. Using these combined strategies, pressure exceeding 150 bars is achieved with minimal penetration loss or leak during a period of 72 h. We demonstrate the success of this high-pressure MAS capability with *in situ* spectra of reaction intermediates and products associated with geochemical studies of deep geological carbon sequestration using the model mineral forsterite (Mg_2SiO_4) reacted with supercritical CO_2 and H_2O at 50 °C and pressure up to 165 bars.

2. Instrumentation

The high-pressure MAS capability consists of three key parts; the high-pressure MAS rotor, the high-pressure rotor loading and reaction chamber, and the MAS probe with localized RF coil [11]. These parts are separately described below.

2.1. The high-pressure MAS rotor

Fig. 1a shows the assembled high-pressure MAS rotor (HP-MAS-R). Fig. 1b highlights the essential components of the HP-MAS-R and the internal matching/fit of the various components. Since the rotor sleeve (OD of 9.5 mm, ID of 8 mm and length of 40 mm), "1", and the drive tip, "2", are commercially available, the outside appearance of the high-pressure rotor resembles that

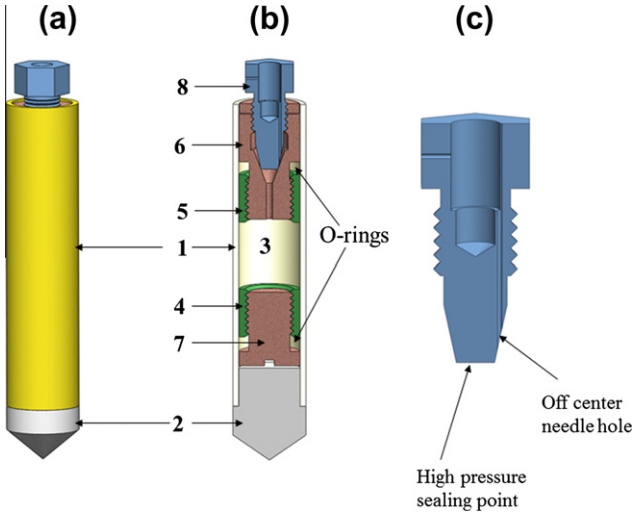

Fig. 1. The high-pressure MAS rotor. (a) The assembled HP-MAS-R; (b) the internal match/fit of the various components; (c) the high-pressure sealing valve.

of a traditional MAS rotor with easy set-up of sample spinning and easy replacement of the rotor sleeve and the drive tip when needed. For our initial experiments, zirconia based ceramic is used for the rotor sleeve and Kel-F is used for the drive tip. Since no plastic inserts are used within the sample cell space, "3", the ^{13}C and ^{1}H background signals are significantly suppressed, which is a significant advantage over prior approaches [9,10]. Another distinct advantage of the present design is the large sample volume, also due to the elimination of the plastic inserts, within the sample cell. For example, using a 9.5 mm rotor, we have achieved an active sample volume of 350 μL, while still maintaining a sample spinning rate of 3.5 kHz and a CO_2 pressure exceeding 150 bars. Since sample spinning introduces a centrifugal force to the rotor sleeve that factors into the overall stress to the rotor when pressurized, the failure or breakdown pressure of the rotor is therefore determined by both the internal fluid pressure and the sample spinning rate.

The centrifugal force of a point mass, F_C, due to spinning is determined by $F_c = m*\omega^2 r = 4\pi^2 * m * f^2 * r$, where m is the mass in units of kg, f is the rotation frequency in Hz, and r in units of meters is the distance between the rotating mass and the center of rotation. Since pressure $P = \frac{F_c}{A}$, where A is the surface area, the centrifugal force can be converted into equivalent pressure. For a thin rotor sleeve with outer radius of R_2, and internal radius of R_1,

$$P = \frac{F_c}{A} \approx \frac{m\omega^2 R_2}{A} = \frac{\left(\pi R_2^2 - \pi R_1^2\right) * \frac{\Delta\theta}{2\pi} * L * \rho * \omega^2 * R_2}{\Delta\theta * R_1 * Ł} = \frac{(R_2 + R_1) * (R_2 - R_1) * \rho * \omega^2 * R_2}{2 * R_1} \quad (1)$$

where ρ is the density of the rotor sleeve, L is the length of the cylinder, $\Delta\theta$ is the angle in radian spanned by the small mass. Eq. (1) denotes the maximum pressure since $R_1 \leqslant R_2$ and $A \geqslant \Delta\theta * R_1 * L$. For zirconia, $\rho = 6.52 \frac{g}{cm^3}$.

The maximum pressure of our HP-MAS-R design is not limited by the zirconia cylinder. We found by pressure failure tests that a standard rotor cylinder based on zirconia ceramic with an OD of 9.5 mm and an ID of 8 mm is capable of withstanding pressures up to 486 bars without breaking. The equivalent pressure due to centrifugal force at a sample spinning rate of, "f", calculated using Eq. (1) and is found to be

$$P_C = \frac{(R_2 + R_1) * (R_2 - R_1) * \rho * \omega^2 * R_2}{2 * R_1} = 0.025405 \frac{g}{mm} * 4\pi^2 f^2 = 1.002952 \frac{g}{mm} f^2 = 1.002952 \frac{kg}{m} f^2 = \frac{1.002952}{100000} f^2 bar \quad (2)$$

where f is in unit of Hz. Hence, at sample spinning rates of 2, 3.5, and 7 kHz, the equivalent pressure due to spinning would be 39.7, 121.6 and 486.6 bars, respectively. If we assume a rotor sleeve break pressure of around 486 bars and a sample spinning rate of 3.5 kHz, the zirconia ceramic rotor itself should be able to withstand about 360 bars of internal pressure. Thus, standard zirconia ceramics are ideal for this application and are not the limiting factor for achieving high-pressure.

A bigger technical challenge is the high pressure seal. In our design, two plastic bushings labeled as "4" and "5" are used at both ends of the rotor sleeve. The interior surface immediately outside the sample cell space "3" of the zirconia sleeve ("1" in Fig. 1a and b, respectively) was roughened up and an epoxy coating was applied [12] in order to tightly glue the bushings "4" and "5" to the interior surface of the zirconia sleeve. Removable plastic end parts (valve-adaptor "6" and end plug "7") were then mounted to the two bushings via screw type of mounting. To tightly seal the cell volume, O-rings are used in between the zirconia sleeve

and removable plastic components as illustrated in Fig. 1b. Since the end plug and the valve adaptor are not glued to the assembly, this design facilitates sample filling (re-filling), sample cell cleaning for reuse, and easy replacement of the O-rings, the end plug, and the valve adaptor when needed. The seal between the valve "8" and the valve-adaptor is realized via the tight contact between the perimeter at one end of the circular surface of the valve and the conical surface of the valve-adaptor as illustrated in Fig. 1b. This type of single point, or very narrow contact surface seal, is widely used in high-pressure fittings. The difference between our design and the standard high-pressure fitting design is the introduction of a needle hole that is drilled off the symmetric axis of the valve as indicated in Fig. 1c. This hole allows high-pressure fluids to pass into the sample cell before the seal is created. Using this design the seal can be created by turning the valve by less than half a turn. Therefore, the volume change of the fluids inside the sample cell before and after the seal is minimal. Consequently, the pressure inside the cell after sealing is essentially the same as the loading pressure, which is very important for accurately setting up experimental conditions before the sample is moved to an NMR probe.

2.2. The high-pressure rotor loading/reaction chamber

The high-pressure rotor loading chamber (HP-RLRC) shown in Fig. 2 is developed for both loading and sealing the high-pressure fluids inside the HP-MAS-R, as well as for re-opening the valve of the HP-MAS-R under pressure for sample access and continued reaction. The main body of the HP-RLRC is constructed from two stainless steel blocks, i.e., the top block in gray color and the bottom block in green, that are held together by eight bolts, each of 7.8 mm diameter and 120 mm long. Between the two blocks two O-rings with sizes 65 × 2.5 mm OD × CS and 50 × 2.5 mm OD × CS are used to make the high-pressure seal. The rotation mechanism for sealing the high-pressure rotor is mounted at the top block while the mechanism for tightly holding the rotor is built at the bottom of the block as highlighted in Fig. 2b and c. After all the components, including the HP-MAS-R, are mounted in place, the net volume for the high-pressure fluids in the loading/reaction chamber is about 9 cm^3. Two horizontal observation windows made of transparent materials such as polycarbonate, quartz or sapphire, are built in the upper block as shown in Fig. 2a and b to facilitate viewing the engagement of the rotating mechanism with the valve of the high-pressure rotor during sealing, or re-opening of the HP-MAS-R. Each of the two windows is held in place by a stainless steel plate with eight bolts. Again O-rings are used for high-pressure seals. Additionally, five input ports with control valves are built in to the upper block, including two fluid inputs and one for releasing pressure after sample loading and/or reaction. A pressure gauge mounted to one port for accurately reporting the pressure inside the chamber, and a thermocouple for accurately recording the fluid temperature at the inner top of the loading/reaction chamber are mounted via two input ports.

The details of the rotation seal mechanism and the mechanism for holding the HP-MAS-R are illustrated in Fig. 2b and c, respectively. The rotation seal mechanism consists of a rotating shaft, stainless steel high-pressure thrust bearing, and two O-rings. A hexagonal hole that matches the hexagonal shape of the valve head (see Fig. 2c) is made at one end of the rotating shaft to allow for engagement of the rotor valve head. The thrust bearing is used to facilitate rotation under high-pressure. The two O-rings, a 60 × 2.5 mm OD × CS and a 40 × 2.5 mm OD × CS, are used to seal the rotation mechanism under high-pressure using a combination of a stainless steel plate and 10 stainless steel screws. The high-pressure rotor is secured in place via an O-ring and a screw cap with the center open to the rotor as indicated in Fig. 2c. After the screw cap is tightened, the O-ring is squeezed tightly against the rotor surface. We found that the friction is adequate to hold the rotor in place during rotation of the shaft. Although the shaft can only undergo rotational motion with no net vertical movement, the valve is driven down to create the required seal by sliding it down vertically inside the matching hole in the rotation shaft as illustrated in Fig. 2c. Two thermocouples are placed close to the sample for accurate measurement of the temperature inside the chamber.

The high-pressure chamber is connected to a primary programmable high-pressure ISCO DM 100 syringe pump [13] that is rated to 500 bars, and a secondary, manually operated HIP piston screw generator [14] with volume of 10 cm^3 that can pressurize up to 4136 bar. A fluid-manifold bench was designed so that mixed gases and/or liquids (depending on pressure and temperature desired) can be loaded into the chamber. The chamber temperature is controlled using a conventional hotplate, Cimarec [15], capable of attaining temperatures of 400 °C. In the future, an oven will be used to replace the heating pad for more uniform heating of the entire HP-RLRC.

The following steps are used to load the sample inside the rotor and to seal the high-pressure fluids. (a) Without the valve-adaptor and the valve in Fig. 1, the sample cell is cleaned and then the sample is loaded in the usual way. (b) After loading the sample, the inner thread of bushing "5" is cleaned of sample powder, followed by mounting the valve-adaptor, and the O-ring. The valve is mounted carefully but not sealed. (c) The rotor assembly is moved into the bottom block of the chamber and tightly mounted (see Fig. 2c). (d) The rotation shaft is aligned with and engages the valve in the HP-MAS-R. (e) High-pressure fluids of desired pressure are introduced into the chamber using the syringe pump assembly discussed above. The needle hole inside the valve of the MAS rotor allows pressure outside and inside the sample cell to equalize within seconds to minutes. After pressure equilibrium is reached, a clockwise turn of the rotation shaft will seal the high-pressure fluid inside the HP-MAS-R. Likewise, an anti-clockwise rotation will open

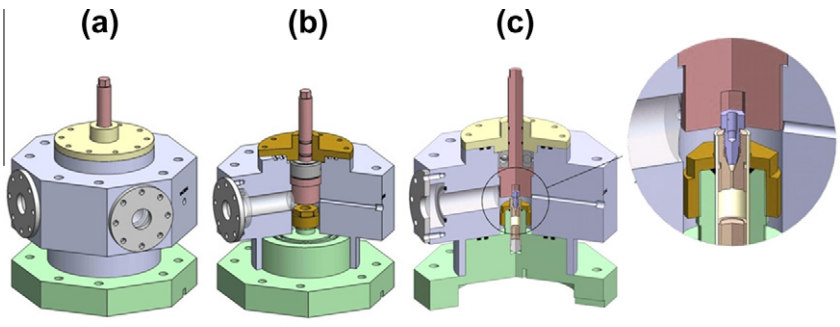

Fig. 2. The high-pressure rotor loading/reaction chamber. (a) External view of the device; (b) dissection view of the rotation mechanism for sealing the high-pressure rotor (top plate of the chamber); and the mechanism for tightly holding the rotor (bottom plate of the chamber); (c) a highlight of the mechanism used for *in situ* closing and opening the valve inside the high-pressure MAS rotor.

the valve and expose the sample cell through the needle hole in the valve to the fluids inside the high-pressure chamber. Opening and closing the valve is most conveniently performed (i.e., with least external force or torque) if the pressure both inside and outside the HP-MAS-R are about the same.

2.3. The large-sample-volume MAS NMR probe

Our large sample volume MAS probe (9.5 mm) with temperature control is of a traditional pencil-type design and was built to operate at a magnetic field of 7.05 T, corresponding to a ^{1}H Larmor frequency of 300 MHz. Since our HP-MAS-R contains plastics at both ends of the sample cell, an RF coil with localized B_1 field such as a saddle-RF coil [16,17] should be employed for minimal ^{13}C and ^{1}H background signals. This is realized initially using a four turn saddle-RF coil (Fig. 3). Using the saddle-RF coil design, a 5.5 μs ^{13}C 90 degree pulse width was obtained using an input power of about 500 W.

3. Performance analysis

3.1. Break pressure of the plastic materials in the high-pressure rotor

Three different materials, i.e., polyether ether ketone (PEEK), high-performance polyimide-based plastics (VESPEL), and polyamide-imides (TORLON), were chosen for constructing the bushing, valve-adapter, valve and the end plug. These plastics were chosen because they are known high performance plastics that are widely used in a variety of high-pressure applications. The valve-adaptor, "6" in Fig. 1, is mounted and tested by replacing the valve, "8", with a standard high-pressure stainless steel fitting having the same geometry as that of the valve. Our tests indicate that the valve-adaptor is the weakest component of the HP-MAS-R. The break point or section in the valve-adaptor is always close to the high-pressure seal contact point due to the extra stress from the valve. Therefore, it is only necessary to test the break pressure of the valve-adaptor. Using helium gas, the average breaking pressures of the valve-adaptors made of various materials were identified (multiple runs) as 393 bar for PEEK, 344 bar for TORLON, and 241 bar for VESPEL, respectively. Based on this result, VESPEL is eliminated as a potential candidate for the valve due to its lowest break pressure. Although the break pressure of PEEK is higher than that of TORLON, severe CO_2 penetration has been reported previously for PEEK [10]. For the present application involving supercritical CO_2, TORLON was chosen as the material for the end plug, the valve-adaptor and the valve of the high-pressure rotor. PEEK was chosen for bushings based on its higher strength, where CO_2 penetration is less of a problem due to the position of the O-ring seal and TORLON valve adapter in our design.

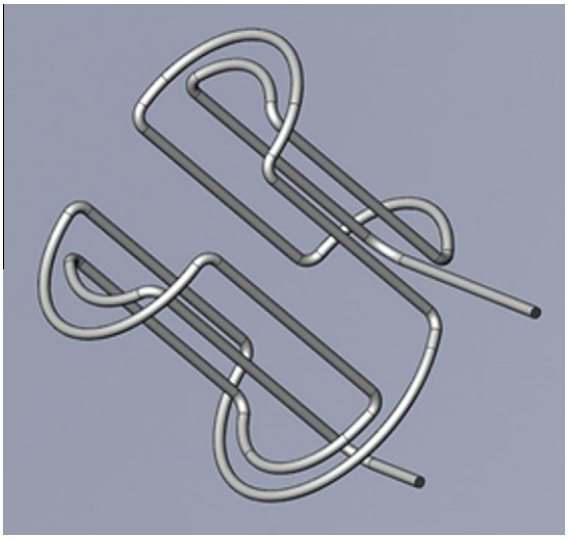

Fig. 3. RF coil with localized B_1 field. The 4 turn saddle-RF coil currently used in the large-sample volume MAS probe.

3.2. Bench test of safety and sample spinning rate

After the rotor is sealed using the high-pressure loading chamber, the rotor is bench tested for sample spinning and safety before loading into an NMR probe. For the test a simple MAS housing without RF coil is placed inside a Tenney Environmental oven with temperature controlled at the same temperature as that of the high-pressure loading/reaction chamber. Cables for MAS bearing and drive gases as well as spinning speed detector and thermocouple are all guided through the oven side wall via an open hole (purposely drilled) so that the temperature of the MAS rotor can be set accurately.

3.3. High-pressure rotor transfer

For safe transfer of the pressurized MAS rotor/sample from the loading chamber to the NMR laboratory, the rotor is placed inside a screw capped stainless steel safety cell. The safety cell, in a cylindrical shape with 8 mm thick wall and 16 mm thick bottom and top caps, keeps the loaded rotor at approximately the same temperature as that of the chamber during loading.

4. Results and discussion

As an example of its many possible applications, the high-pressure MAS capability is here applied to understanding fundamental mineral carbonation reaction mechanisms associated with geological carbon sequestration (GCS), where CO_2 is injected and stored in geologic formations [18–21] at depths where lithostatic pressure maintains the CO_2 in a supercritical fluid state ($scCO_2$). The pressure, temperature and the density at the critical point of CO_2 are 73.825 bar, 31.06 °C and 0.466 g/cm^3, respectively [22]. If employed at large-scales, GCS represents one of the most promising options for mitigating the impacts of greenhouse gases on global warming owing to the potentially large capacity of prospective geologic formations and their broad regional availability [18–21]. A critical issue is to demonstrate that CO_2 will remain stored over the long-term in the host rock where it is injected. In this regard, mineral-fluid interactions are of prime importance because such reactions can result in the long term sequestration of CO_2 by trapping in mineral phases as metal carbonates [23–26]. However, currently little is known about the mechanisms of metal carbonation associated with GCS in $scCO_2$ and mixed CO_2–H_2O fluids, and their study presents unique challenges due to the highly corrosive nature of $scCO_2$ containing H_2O. To help address this problem, *in situ* analytical tools are needed that are able to provide molecular level information on reaction rates. The high-pressure MAS capability developed in this work is ideally suited for these kinds of investigations. In the following, results obtained from select studies are reported to demonstrate the functionality and performance of our high-pressure MAS capability.

Forsterite, i.e., Mg_2SiO_4, is used as the reactant mineral. As-received Mg_2SiO_4 from Alfa Aesar was oven dried at 200 °C for 12 h before it was loaded into the HP-MAS-R. For the investigation, research grade 99% ^{13}C labeled CO_2 gas (Cambridge Isotope Laboratories) was mixed with high purity natural abundance CO_2 at a ratio of 1:6, corresponding to a net isotope enrichment of 14.3%. All the ^{13}C NMR measurements were performed on a Agilent-Varian

300 MHz VNMRS spectrometer at 75.44 MHz Larmor frequency using a single pulse (SP) sequence.

Fig. 4a shows a ^{13}C SP-MAS spectrum of natural abundance $scCO_2$ at a pressure of 130 bars and a temperature of 50 °C using a sample spinning rate of 1.7 kHz. This spectrum was acquired without ^{1}H high power decoupling using a total of 1600 scans with a recycle delay time of 1 s. Exponential apodization in the time domain equivalent to a line broadening of 40 Hz was applied prior to Fourier transformation so that the background signal can be clearly shown. Without line broadening the linewidth of the CO_2 peak located at about 126.0 ppm is about 15.6 Hz. The background peak arising from the Viton® O-rings [27] is centered at about −2 ppm and is of very low intensity as indicated by the 32 fold vertically expanded inset spectrum between −50 and 50 ppm. With ^{1}H high power decoupling applied, background signals from the bushings, the plugs, the valve and the valve adaptors can be observed and are depicted in Fig. 4b. Note that for acquiring Fig. 4b, no CO_2 is loaded in the rotor. Even with 7200 scans and a recycle delay time of 2 s, the background signal is quite weak. These results demonstrate that sufficient B_1 localization has already been achieved by a combination of the elimination of plastic inserts within the sample cell and the saddle RF coil in the 9.5 mm MAS probe.

Leakage test results of the HP-MAS-R at 50 °C (323 K) with an initial $scCO_2$ pressure of 150 bars are summarized in Fig. 5. Fig. 5a shows the integrated ^{13}C peak intensity of $scCO_2$ (with peak maximum at 126.0 ppm) as a function of the holding time at a sample spinning rate of 1.64 kHz. The decay of the signal is approximately linear with time. About 81% of the peak intensity remains even at a holding time of 72 h. To determine whether the CO_2 is at supercritical conditions over the course of the experiment, the density of the CO_2 needs to be determined first. It is known that for a pressure of 150.0 bar, the CO_2 density is 0.727 g/cm^3 at 320.0 K and 0.636 g/cm^3 at 330.0 K, respectively [22]. Using linear extrapolation, the CO_2 density at 150.0 bar and 323.0 K was determined to be 0.70 g/cm^3. Since the integrated spectral intensity of the CO_2 peak is directly proportional to the CO_2 density inside the fixed volume sample cell of the high-pressure rotor, the expected density of CO_2 as a function of holding time at 323.0 K can be obtained by multiplying the percentage of the CO_2 peak intensity remaining and the assumed initial CO_2 density of 0.70 g/cm^3. The results are plotted in Fig. 5b. To validate the density data in Fig. 5b, a separate experiment was carried out by sealing HP–MAS-R *in situ* at the same conditions of 150 bar $scCO_2$ and 50 °C. The sample volume of the HP-MAS-R used was determined as 0.28 ± 0.01 cm^3 using the standard method of filling H_2O inside the sample cell. Immediately after moving the sealed HP-MAS-R out of the high-pressure loading chamber, the weight of the CO_2 inside the MAS rotor was obtained as 0.189 g. This corresponds to an initial CO_2 density of approximately 0.68 g/cm^3, which is within the experimental error range to the expected CO_2 density of 0.70 g/cm^3 at 150 bar and 50 °C. The sealed HP-MAS-R was then spun at 1.64 kHz inside a 50 °C oven and periodically taken out to record the weight of the rotor assembly, i.e., determining the density of the CO_2 inside the rotor. Density data obtained during a time period of 27 h are included in Fig. 5b for comparison with the expected values obtained from the *in situ* ^{13}C MAS NMR measurements. The data obtained from periodically weighing the sample rotor closely match the data from the *in situ* ^{13}C MAS experiment, confirming the density data obtained from the NMR measurement. Using the data from Ref. [22], the CO_2 density at supercritical conditions, i.e., 73.8 bar and 323.0 K, is 0.190 g/cm^3. It is known from Fig. 5b that the CO_2 density at a holding time of 72 h at 323.0 K is 0.565 g/cm^3. Because the CO_2 density is 0.407 g/cm^3 at 100.0 bar and at 323.0 K, and 0.700 g/cm^3 at 150 bar and at 323.0 K, respectively, a CO_2 density of 0.565 g/cm^3 at 323.0 K corresponds to a CO_2 pressure of approximately 126.9 bar [22]. Therefore, the results in Fig. 5b clearly indicate that $scCO_2$ conditions inside the HP-MAS-R are maintained over the course of the measurement.

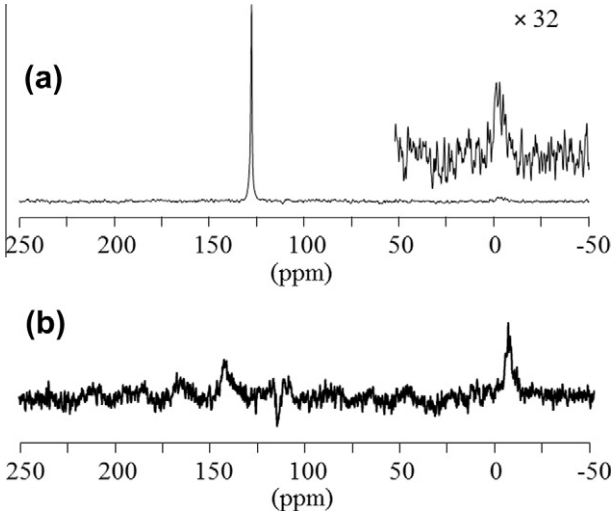

Fig. 4. Background test, illustrating the low ^{13}C background achieved. ^{13}C SP-MAS spectrum of natural abundance $scCO_2$ at a pressure of 130 bars, a temperature of 50 °C, and a sample spinning rate of 1.7 kHz. A pulse width of 4 μs, corresponding to a ~65° pulse angle was used A Lorentz line broadening of 40 Hz was used before Fourier transformation. (a) Without ^{1}H high power decoupling; (b) with ^{1}H high power decoupling (~50 kHz) applied. The number of accumulations and the recycle delays used were 1600 and 1 s for (a), 7200 and 2 s for (b), respectively.

Fig. 6 summarizes *in situ* ^{13}C SP-MAS NMR studies on Mg_2SiO_4 reacted with $scCO_2$ and H_2O. The reaction conditions were as follows. Using a needle syringe, approximately 0.1 g of H_2O was injected into the center of the sample cell inside the HP-MAS-R that was pre-loaded with 0.27 g of dry Mg_2SiO_4 powder. The rotor valve was then closed and mounted inside the high-pressure loading chamber, followed by pressurizing the loading chamber to 150 bar with 14.3% ^{13}C enriched CO_2, and by raising the temperature to 50 °C. Shortly after the reaction conditions (both targeted pressure and temperature) were stabilized, the rotor valve was opened to allow chamber $scCO_2$ to fill the sample cell containing the mineral and water, and the reaction was carried out for 50 h. To ensure that the H_2O inside the HP-MAS-R remains inside the sample cell and in contact with the forsterite powder to form a liquid H_2O film on the forsterite surface during CO_2 pressurization and during the reaction (as opposed to being desiccated out of the rotor by the chamber CO_2), an additional 1 mL of excess bulk water (not in direct contact with minerals) was pre-added into the bottom of the high-pressure loading chamber. Because the CO_2 is buoyant relative to the water, the water remains in the bottom of the chamber to act as the main H_2O source for saturating the $scCO_2$ before the rotor valve was opened.

It is known that for a given fluid/mineral ratio there is a H_2O film thickness threshold, about 18 nm, above which a significant portion of the H_2O serves in a catalytic role where more extensive carbonation reaction occurs [28]. Using BET, the initial surface area of the forsterite powder was determined to be 1.00 m^2/g. To simplify the discussion, if we assume that the 0.10 g H_2O in contact with the 0.27 g forsterite powder forms a homogeneous H_2O film on the mineral surface, the corresponding initial H_2O thickness would be about 370 nm. A H_2O film of 370 nm is well above the H_2O film threshold, a condition suitable for demonstrating the high-pressure MAS capability where H_2O serves as a catalyst and the reaction would last for a long period of time. It is also likely that in this experiment, excess water beyond saturation of the $scCO_2$ trapped in the rotor condensed to form a relatively minor liquid water phase in the rotor in contact with the forsterite.

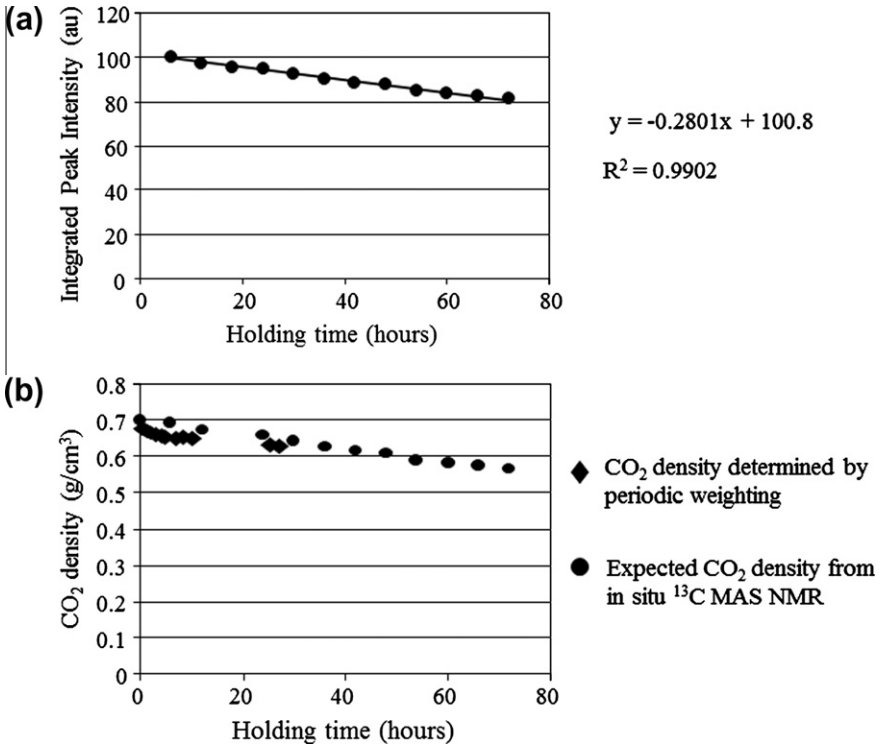

Fig. 5. Leakage test of the HP-MAS-R at an initial pressure of 150 bars and at 50 °C. (a) The integrated peak intensity of the ^{13}C SP-MAS spectrum of CO_2 as a function of holding time. The spectrum corresponding to each data point was acquired using a recycle delay time of 20 s and an accumulation number of 200. Thus each point is the result of about 1 h data average. Other experimental conditions were similar to those in Fig. 4b; (b) "•" The estimated CO_2 density in the sample cell of the HP-MAS-R as a function of holding time obtained from the *in situ* ^{13}C MAS NMR measurements, "♦" The CO_2 density estimated by periodically weighing the HP-MAS-R (see text for details).

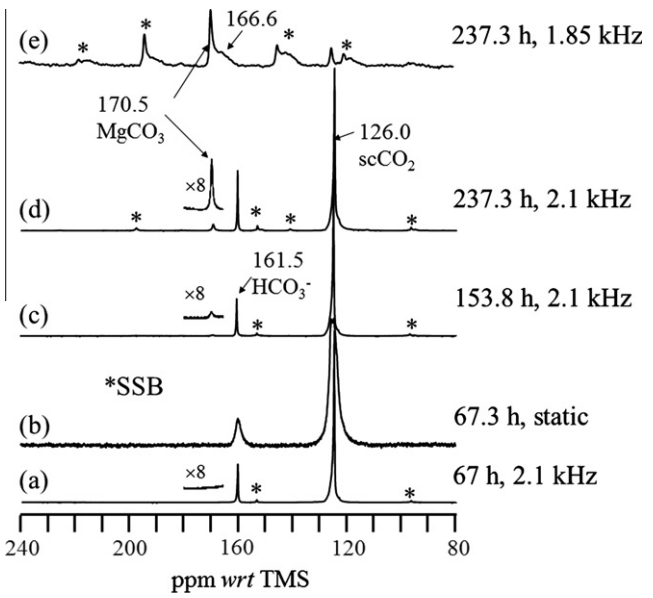

Fig. 6. *In situ* ^{13}C SP-MAS NMR spectra acquired at a sample spinning rate of 2.1 kHz on 0.27 g Mg_2SiO_4 + 0.1 g of H_2O + 150 bar 14.3% ^{13}C enriched CO_2 + 1 g of extra H_2O separated from the forsterite powder at 50 °C for 67.3 h (including 17.3 h acquisition time) (a), 153.8 h (including 25 h second acquisition time period) (c) and 237.3 h (including 22 h third acquisition time period) (d), respectively. (b) Static spectrum acquired immediately after (a). (e) MAS spectrum after (d) and after the $scCO_2$ was released. Spinning side bands (SSB) are labeled by "∗". The accumulation numbers were 20386 (a), 140 (b), 30,134 (c), 26,759 (d), 165,000 (e), respectively. All other experimental conditions were similar to those in Fig. 5a. The integrated peak area for the $MgCO_3$ normalized to per unit number of accumulation increase by 6.4 fold from (c) to (d).

At the end of the desired reaction time, the MAS rotor was sealed by closing the valve while inside the high-pressure loading chamber and the pressure of the loading chamber was then released. The sealed HP-MAS-R was transported using the 50 °C preheated-sample safety cell to the MAS probe that was also preheated to 50 °C for measurements. The corresponding *in situ* ^{13}C MAS NMR spectra, acquired at a spinning rate of 2.1 kHz, shows only two isotropic peaks located at 126.0 ppm and 161.5 ppm, respectively (Fig. 6a). Like the $scCO_2$ peak at 126.0 ppm, the peak at 161.5 ppm is characterized by a narrow linewidth of 13.3 Hz, and the associated sample spinning sidebands are of very low intensity, indicating highly mobile species. The high mobility of the species for the 161.5 ppm peak is further confirmed by the similar static linewidth of the 161.5 ppm peak compared to that of the 126.0 ppm $scCO_2$ peak (Fig. 6b). Fig. 6b also highlights the importance of magic angle sample spinning for resolution enhancement as the peaks are significantly broadened in the static spectrum due to the magnetic susceptibility gradients in this heterogeneous mixing system even for these highly mobile species. It is known [29] that the chemical shift values of HCO_3^- and H_2CO_3 are 161.2 ppm and 162.9 ppm, respectively. With confidence the 161.5 ppm peak is assigned to HCO_3^-.

Although there was a considerable amount of $scCO_2$ inside the HP-MAS-R, most of the sample cell (more than 50%) is filled with forsterite powder. Therefore, the *in situ* HP-MAS-R is perhaps better viewed in this case as an *in situ* sampling device rather than an *in situ* reactor.

To continue the reaction (after the initial 50 h of reaction and 17.3 h acquisition time), the HP-MAS-R was returned to the HP-RLRC (pre-heated at 50 °C), followed by re-equilibrating the chamber to 150 bars. The time for the re-equilibrium took about 1.5 h. The rotor valve was then re-opened and the reaction was thereby allowed to continue, in this case for an additional 60 h, and then the rotor valve was closed for removal and NMR analysis. The total reaction time was thus 153.8 h, including the first experiment of

67.3 h, the 1.5 h for pressure re-equilibrium, and 25 h second acquisition time. A third peak centered at 170.5 ppm was then observed in the corresponding *in situ* 2.1 kHz ^{13}C SP-MAS spectrum (the 8 times vertically expanded inset in Fig. 6c). By returning the HP-MAS-R to the HP-RLRC for a third time for an additional 60 h of reaction, *in situ* ^{13}C SP-MAS spectra at a cumulative reaction time of 237.3 h were also obtained (Fig. 6d). Clearly, the intensity of the 170.5 ppm peak increases with the reaction time. The full width at half maximum (FWHM) (50.3 Hz) of the 170.5 ppm peak is much broader than that of the 161.5 ppm or the 126.0 ppm peaks. Furthermore, there are strong spinning sidebands at a spinning rate of 2.1 kHz, indicating that the 170.5 ppm peak arises from a solid phase. It has been reported previously [30] that the ^{13}C chemical shift of magnesite ($MgCO_3$) is at 170.2 ppm. Therefore, the 170.5 ppm peak is correspondingly assigned to the forsterite carbonation product magnesite. This identification was further confirmed by performing a ^{13}C SP-MAS experiment (Fig. 6e) on the same sample, where the CO_2 was released shortly after acquiring Fig. 6d and then the sample was stored at ambient conditions for 13 days before acquiring Fig. 6e. It should be pointed out that each spectrum was an averaged spectrum across the data acquisition time where some reaction would occur.

In this sequence it was intriguing to discover that the HCO_3^- peak at 161.5 ppm disappeared together with the $scCO_2$ peak at 126.0 ppm. Careful evaluation of Fig. 6e reveals a shoulder peak located at about 166.6 ppm that has been previously assigned to hydrated/hydroxylated magnesium carbonates, an intermediate phase to magnesite, such as hydromagnesite, dypingite, and nesquehonite ($MgCO_3{\cdot}3H_2O$) based on ex situ NMR studies [28]. Because the metal carbonation product, i.e., $MgCO_3$ is not observed before the full appearance of the HCO_3^- peak, HCO_3^- is thus a key reaction component.

To differentiate whether HCO_3^- is associated with the $scCO_2$ or the H_2O phase/H_2O film on the forsterite surface, the following two experiments were carried out. In the first experiment, the HP-MAS-R was filled with forsterite powder as before and 0.10 g H_2O and then pressurized to 165 bar with 14.3% ^{13}C $scCO_2$ at 50 °C while inside the high-pressure loading chamber that was loaded with a 1 mL excess H_2O pool as previously described. After a reaction time of 2 h, the HP-MAS-R was sealed *in situ*. The corresponding *in situ* ^{13}C SP-MAS results are given in Fig. 7a. Clearly, both the 161.5 ppm and the 126.0 ppm peaks are observed. Observation of an intense HCO_3^- signal at a reaction time of only 2 h suggests that the reaction of $scCO_2$ with H_2O to form HCO_3^- is rapid compared with the process of metal carbonation (Fig. 6). After acquiring the spectrum in Fig. 7a, the CO_2 pressure was incrementally released by using the high-pressure loading chamber to step the pressure down to 65.0, 5.0, and 2.5 bars, sequentially. The ^{13}C SP-MAS spectrum at each CO_2 pressure step was acquired. Clearly the 161.5 ppm peak remains visible albeit its relative intensity is decreased as the CO_2 pressure is gradually released, i.e., from 1.0 (165.0 bar), to 0.42 (65.0 bar), to 0.27 (5.0 bar), to 0.25 (2.5 bar). However, the intensity of the CO_2 peak decreases much faster than that of the HCO_3^- peak, indicating that the HCO_3^- is a dissolved species associated with a minor liquid water phase. To further confirm this conclusion, a second experiment was carried out under the same experimental conditions as the first except no H_2O was loaded directly into the HP-MAS-R. In this case, only the 126.0 ppm $scCO_2$ peak is observed, confirming that HCO_3^- is only associated with the H_2O phase.

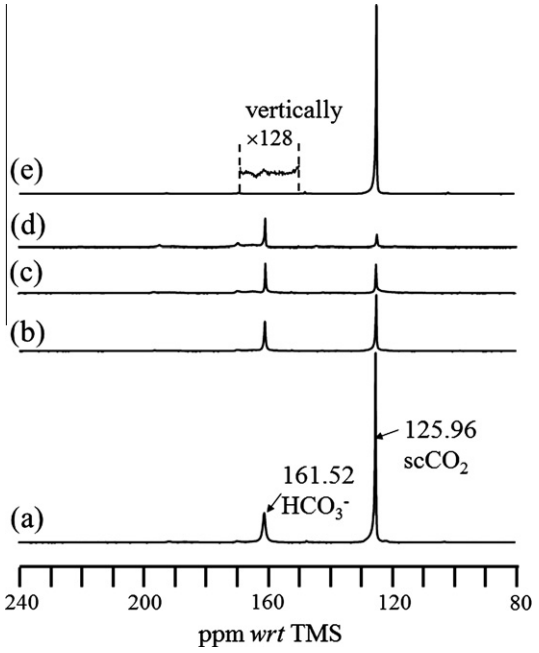

Fig. 7. ^{13}C MAS spectra acquired at a sample spinning rate of 1.85 kHz on the sample of 0.224 g of H_2O + 165 bar 14.3% ^{13}C enriched $scCO_2$ + 1 g of extra H_2O in the reaction chamber that was separated from the sample cell of the MAS rotor (a–d). The volume of the sample cell was about 312 μl. Thus the net volume of the wet $scCO_2$ phase was about 88 μl. The reaction temperature was 50 °C for 2 h. (a–d) were acquired sequentially by reducing the pressure inside the MAS rotor. (a) 165.0 bar at 50 °C; (b) 65.0 bar at 50 °C; (c) 5.0 bar at 50 °C; and (d) 2.5 bar at 50 °C. The number of accumulations was 4000 (a), 20,000 (b), 40,000 (c), and 30,000 (d), respectively, with a recycle delay time of 2 s. (e) ^{13}C MAS spectrum acquired on 165 bar 99% ^{13}C enriched $scCO_2$ + 1 g of extra H_2O in the reaction chamber that was separated from the sample cell of the MAS rotor. The reaction temperature was 50 °C for 2 h. This spectrum was acquired using a sample spinning rate of 1.7 kHz and an accumulation number of 7500 with a recycle time of 2 s. All other experimental conditions for (a–e) were similar to those in Fig. 5a.

5. Conclusions

In this work, a high-pressure MAS NMR capability, consisting of a high-pressure MAS rotor (HP-MAS-R), a high-pressure rotor loading/reaction chamber (HP-RLRC), and a MAS probe, is reported. Several technical challenges associated with design and implementation of a reusable HP-MAS-R have been overcome using a custom zirconia ceramic rotor cylinder including abrading the internal surface of both ends for successful high-strength seals with high-pressure plastic end cap materials. Using this design, an internal CO_2 pressure exceeding 150 bars was achieved with minimal loss of pressure during a period of 72 h. The high-pressure sample loading chamber itself is a high-pressure reaction device that is equipped with temperature control and viewing windows, and is specifically designed for both sealing *in situ* and opening *in situ* of the HP-MAS-R valve. In this way, sustained reaction under controlled high-pressure and temperature conditions can be carried out for long periods of time by repeatedly returning the rotor assembly to the high-pressure loading/reaction chamber. *In situ* NMR is carried out by sealing the rotor under pressure in the chamber and then removing it to ambient pressure conditions for transfer and measurement in the NMR probe. This implementation can thus be viewed as a snap-shot of the reaction at the same pressure and temperature conditions as those in the high-pressure loading/reaction chamber. To avoid the background NMR signals arising from the plastic sealing components at the both ends of rotor, the RF coil of the probe generates a localized B_1 field. In our current design, a simple saddle RF coil is used. Improvement of the B_1 localization to the sample cell might be achieved by using thin cylindrical shields at both ends of the saddle RF coil; implementation of this strategy is currently under way in our laboratory.

To demonstrate the utility of this high-pressure MAS capability, *in situ* ^{13}C MAS NMR studies of forsterite (Mg_2SiO_4) carbonation by

supercritical CO_2 mixed with H_2O were carried out at 150 bars and 50 °C. The results clearly show progression of the carbonation reaction from solid phase reactants to solid-phase products, and implicate HCO_3^- as a key reaction species associated with a water phase/H_2O film present in our experiments. Reaction agents, intermediates, and products, regardless of whether they are in gaseous, supercritical fluid, liquid, or solid phases, are all observed in a single *in situ* ^{13}C MAS experiment, offering a significant experimental advantage over the analogous ex situ NMR measurement, where in our case $scCO_2$ and HCO_3^- would not be observable.

Acknowledgments

This research was supported by the Carbon Sequestration Initiative (CSI) funded by Laboratory Directed Research and Development (LDRD) at Pacific Northwest National Laboratory (PNNL), and by the US Department of Energy (DOE), Office of Basic Energy Sciences through a Single Investigator Small Group Research (SISGR) grant. The research was performed using the Environmental Molecular Sciences Laboratory (EMSL), a national scientific user facility sponsored by the Department of Energy's Office of Biological and Environmental Research and located at PNNL. We are grateful to Karl Mueller for helpful discussions.

References

[1] F. Bloch, W.W. Hansen, M. Packard, Nuclear induction, Phys. Rev. 69 (1946) 127.
[2] E.M. Purcell, H.C. Torrey, R.V. Pound, Resonance absorption by nuclear magnetic moments in a solid, Phys. Rev. 69 (1946) 37.
[3] E.R. Andrew, A. Bradbury, R.G. Eades, Nuclear magnetic resonance spectra from a crystal rotated at high speed, Nature 182 (1959) 1659.
[4] I.J. Lowe, Free induction decays of rotating solids, Phys. Rev. Lett. 2 (1959) 285.
[5] M.G. Pravica, I.F. Silvera, Nuclear magnetic resonance in a diamond anvil cell at very high pressures, Rev. Sci. Instrum. 69 (2) (1998) 479–484.
[6] T. Miyoshi, K. Takegoshi, T. Terao, ^{13}C High-pressure CPMAS NMR characterization of the molecular motion of polystyrene plasticized by CO_2 gas, Macromolecules 30 (21) (1997) 6582–6585.
[7] T. Miyoshi, K. Takegoshi, T. Terao, Effects of Xe Gas on segmental motion in a polymer blend as studied by ^{13}C and ^{129}Xe high-pressure MAS NMR, Macromolecules 35 (1) (2002) 151–154.
[8] T. Miyoshi, K. Takegoshi, T. Terao, ^{129}Xe nmr study of free volume and phase separation of the polystyrene/poly(vinyl methyl ether) blend, Polymer 38 (21) (1997) 5475–5480.
[9] C.R. Yonker, J.C. Linehan, The use of supercritical fluids as solvents for NMR spectroscopy, Prog. Nucl. Magn. Reson. Spectrosc. 47 (2005) 95–109.
[10] T. Deuchande, O. Breton, J. Haedelt, E. Hughes, High-pressure magic angle spinning, J. Magn. Reson. 183 (2006) 178–182.
[11] D.W. Hoyt, J.A. Sears, R.V.F. Turcu, K.M. Rosso, J.Z. Hu, A method for high-pressure magic angle spinning nuclear magnetic resonance. US Patent and Trademark office – Patent Pending, November 4, 2010.
[12] S. Bai, C.M. Taylor, C.L. Mayne, R.J. Pugmire, D.M. Grant, A new high-pressure sapphire nuclear magnetic resonance cell, Rev. Sci. Instrum. 67 (1) (1996) 240–243.
[13] ISCO DM100, Teledyne Isco, Inc., Lincoln, NE, 68504.
[14] High-pressure Generator, High-pressure Equipment Company, Erie, PA, 16505.
[15] Cimarec, Thermo Fisher Scientific, Inc., Waltham, MA 02454.
[16] D.I. Hoult, R.E. Richards, The signal-to-noise ratio of the nuclear magnetic resonance experiment, J. Magn. Reson. 24 (1976) 71–85.
[17] D.W. Alderman, D.M. Grant, An efficient decoupling coil design which reduces heating in conductive samples in superconducting spectrometer, J. Magn. Reson. 36 (1979) 447–451.
[18] S. Bachu, Sequestration of CO_2 in geological media in response to climate change: road map for site selection using the transform of the geological space into the CO_2 space, Energy Convers. Manage. 43 (1) (2002) 87–102.
[19] S. Bachu, J.J. Adams, Sequestration of CO_2 in geological media in response to climate change: capacity of deep saline aquifers to sequester CO_2 in solution, Energy Convers. Manage. 44 (20) (2003) 3151–3175.
[20] S. Bachu, CO_2 storage in geological media: role, means, status and barriers to deployment, Prog. Energy Combust. 34 (2) (2008) 254–273.
[21] S.M. Benson, T. Surles, Carbon dioxide capture and storage: an overview with emphasis on capture and storage in deep geological formations, Proc. IEEE 94 (10) (2006) 1795–1805.
[22] S. Angus, B. Armstrong, K.M. deRuck (Eds.), International Thermodynamic Tables of the Fluid State – Carbon Dioxide, Pergamon, Oxford, New York, Toronto, Sydney, Paris, Frankfut, 1976.
[23] J.P. Kaszuba, D.R. Janecky, M.G. Snow, Carbon dioxide reaction processes in a model brine aquifer at 200 °C and 200° bars: implications for geologic sequestration of carbon, Appl. Geochem. 18 (7) (2003) 1065–1080.
[24] J.P. Kaszuba, D.R. Janecky, M.G. Snow, Experimental evaluation of mixed fluid reactions between supercritical carbon dioxide and NaCl brine: relevance to the integrity of a geologic carbon repository, Chem. Geol. 217 (3–4) (2005) 277–293.
[25] K. Pruess, T.F. Xu, J.A. Apps, J. Garcia, Numerical modeling of aquifer disposal of CO_2, SPE J. 8 (1) (2003) 49–60.
[26] T. Xu, J.A. Apps, K. Pruess, H. Yamamoto, Numerical modeling of injection and mineral trapping of CO_2 with H_2S and SO_2 in a sandstone formation, Chem. Geol. 242 (3–4) (2007) 319–346.
[27] DuPont Performance Elastomers L.L.C., Wilmington, DE, 19809.
[28] J.H. Kwak, J.Z. Hu, R.V.F. Turcu, K.M. Rosso, E.S. Ilton, C. Wang, J.A. Sears, M.H. Engelhard, A.R. Felmy, D.W. Hoyt, The role of H_2O in the carbonation of forsterite in supercritical CO_2, Int. J. Greenhouse Gas Control, 10.1016/j.ijggc.2011.05.013.
[29] G. Rasul, V.P. Reddy, L.Z. Zdunek, G.K.S. Prakash, G.A. Olah, Chemistry in superacids. 12. Carbonic acid and its mono- and diprotonation: NMR, ab initio, and IGLO investigation, J. Am. Chem. Soc. 115 (6) (1993) 2236–2238.
[30] J.H. Kwa, J.Z. Hu, D.W. Hoyt, J.A. Sears, C. Wang, K.M. Rosso, A.R. Felmy, Metal carbonation of forsterite in supercritical CO_2 and H_2O using solid state ^{29}Si, ^{13}C NMR spectroscopy, J. Phys. Chem. C 114 (9) (2010) 4126–4134.